Plastic collapse load numerical evaluation of welded beam-to-column steel joints

P. Fuschi, A. A. Pisano, R. Pucinotti

University Mediterranea of Reggio Calabria
via Melissari, I-89124 Reggio Calabria, Italy

Abstract

A finite element based numerical procedure for predicting the plastic collapse load as well as the plastic collapse mechanism of beam-to-column steel joints is presented. The promoted procedure is based on two methods following the static and the kinematic approach of limit analysis. Both methods have been rephrased for a von Mises type material in the deviatoric plane and in terms of deviatoric stress invariants. The key concepts are: i) in the static formulation, to mimic the stress redistribution arising within a structure approaching its critical (collapse) state, being such stresses in equilibrium with the maximum redistributable loads; ii) in the kinematic formulation, to build a plastic collapse mechanism characterized by compatible strain and displacement rates corresponding to a minimum value of loads doing positive work equal to the total plastic dissipation. A validation of the numerical results is pursued by comparison with experimental findings on real scale prototypes of the tackled steel joints. Future developments are outlined at closure.

Keywords: Numerical limit analysis, Welded steel joints, Computational modelling, Experimental validation.

1. Research context, motivations and main goals

The structural analysis of steel joints is nowadays a matter solved by any commercial numerical code in the engineering fields. Both the constitutive behaviour of steel and the post-elastic behaviour of steel structural components are successfully described by commercial finite element (FE) codes in statics or in dynamics also in presence of damaging processes. Sophisticated step-by-step and/or time-stepping algorithms are available robust tools to handle the analysis of steel structures. Also the accuracy and computational performance of such algorithms, when dealing with only-steel elements, is certainly the more competitive. So that, the here claimed evaluation of the plastic collapse load for welded beam-to-columns steel joints, avoiding the description of the post-elastic behaviour of the addressed steel structural elements, might appear even outdated.

The problem here in mind is however related to the use of those steel structural components as parts of more complex structural systems characterized by the presence of other structural elements made of materials whose constitutive as well as post-elastic behaviour is not easy to handle or it is described by criteria not possessing the necessary general applicability. This is actually a recurrent circumstance when dealing, for example, with seismic retrofitting of masonry or reinforced concrete existing structures often pursued by strengthening techniques which insert moment resistant steel frames or steel bracing systems, see e.g. [1], [2], [3], [4] and references therein. A similar circumstance appears also in composite steel-concrete structures, [5], [6], or in new composite steel-concrete structural elements as, for example, in concrete filled welded steel columns [7], [8], [9], [10] or in steel ribs for

strengthening of steel concrete joints [11], or in composite beams [12], also in presence of other materials of common use nowadays as fiber reinforced polymers [13].

The above list of papers, far to be exhaustive, gives the idea of the research context hereafter referred in which a conflict in the adoptable design methodologies arises. From one side, steel members and their mutual joints are described by well known constitutive criteria, as von Mises for example, and can be handled by plasticity or damage theories fully implemented in nonlinear FE codes. From the other side, structural elements made of masonry or concrete, whose constitutive as well as post-elastic behaviour is not uniquely defined being also affected by the constructive techniques, are often treated with FE codes whose results are valid only for very particular cases or structural typologies. In this context a direct method, as Limit Analysis, with all its congenital limitations, can result more reliable to predict a limit load of plastic collapse for steel members and of rupture for the other ones giving rise to a complete and effective limit states design approach.

The present work finds and tries motivations on the above considerations and, as a first step of the study, presents a limit analysis FE based procedure applied to steel joints. It is worth noting that, looking at a real engineering practical context, limit analysis has to be performed numerically, indeed a FE based friendly procedure is presented in the paper while the joints are focused being the weak points of a steel elements system. The promoted method, already experienced by the authors in different contexts [14], [15], [16], [17], [18], is here applied to welded beam-to-column joints to predict their plastic collapse load. Perfect associative plasticity is postulated and von

Mises yield criterion in deviatoric plane is used throughout. Two different numerical techniques, based on the static and the kinematic approach of limit analysis respectively, are simultaneously applied to detect the plastic collapse limit load of the analyzed joints. The procedure and the related numerical findings are validated by comparison with experimental outputs on real scale prototypes, [19], to show the robustness and reliability of the numerical plastic limit state design when facing a real engineering problem.

2. Limit analysis via a FE-based procedure

2.1. Theoretical bases

In the realm of perfect plasticity, limit analysis gives the theoretical tools to determine the plastic collapse loads, i.e. the loads under which the structure, modeled as elastic-perfectly plastic, reaches a *critical state* in which large increases in plastic deformation become possible with little, if any, increase in loads.

For simplicity, but without loss of analytical rigor and practical effectiveness, in the following the loads are only the external surface actions applied to the structure, body forces are assumed negligible with respect to the formers. Moreover, as usual in this context, all the acting loads are expressed in terms of assigned reference loads, say $\bar{\mathbf{p}}$, multiplied by a single load multiplier, say P. To set the problem from an analytical point of view, let us now denote with V the volume, referred to a $3D$ Euclidean space, occupied by the analyzed structure whose external surface is $S = S_t \cup S_u$ where S_t is the portion where loads $P\,\bar{\mathbf{p}}$ act and S_u the portion where boundary kinematic conditions, say $\mathbf{u} = \bar{\mathbf{u}}$, are specified.

The cited theoretical tools are the well known *theorems of limit analysis*, based on the principle of maximum plastic dissipation valid only for standard materials as the one here assumed, and furnishing a lower bound, P_{LB}, and an upper bound, P_{UB}, to the plastic collapse load multiplier, say P_U. Borrowing from a classis textbook on plasticity, [20], the two theorems may be stated as follows:

Static or Lower bound theorem: the loads that are in equilibrium with a stress field that nowhere violates the yield criterion do not exceed the collapse loads. That is, if at every point within V exists a stress field $\tilde{\sigma}_j$ with $f(\tilde{\sigma}_j) \leq 0$, with j ranging over the components of the stress vector in principal stress space and $f(\sigma_j)$ denotes the yield function in the same space, and also the stress field $\tilde{\sigma}_j$ is in equilibrium with the applied loads $P_{LB}\,\bar{\mathbf{p}}$, then P_{LB} is a lower bound to the plastic collapse load multiplier P_U, i.e. $P_{LB} \leq P_U$.

Kinematic or Upper bound theorem: the loads that do positive work on a kinematically admissible velocity field at a rate equal to the total plastic dissipation are at least equal to the collapse loads. That is, if the acting loads are $P_{UB}\,\bar{\mathbf{p}}$; $\dot{\mathbf{u}}^c$ is a kinematically admissible velocity field whose related compatible strain rates, say $\dot{\varepsilon}^c_j$, have the direction of the outward normal to the yield surface $f(\sigma_j) = 0$ at $\sigma_j = \sigma^Y_j$, which means that $\dot{\varepsilon}^c_j = \dot{\lambda}\,(\partial f/\partial \sigma_j)$ with $\dot{\lambda} > 0$ being a scalar multiplier; σ^Y_j denotes the stresses at yield associated to $\dot{\varepsilon}^c_j$, then P_{UB} given by

$$P_{UB} = \frac{\int_V \sigma^Y_j\, \dot{\varepsilon}^c_j\, dV}{\int_{S_t} \bar{p}_i\, \dot{u}^c_i\, dS_t} \tag{1}$$

is an upper bound to the plastic collapse load multiplier P_U, i.e. $P_{UB} \geq P_U$.

It is well known that for standard materials the maximum value of P_{LB}

and the minimum value of P_{UB} produced by the application of the two theorems are equal to each other and they also equal the collapse load multiplier P_U. The static and the kinematic approaches of limit analysis pursued to detect P_U are essentially techniques to maximize P_{LB} and to minimize P_{UB}, respectively. The above theorems, as well as the limit analysis approaches they generate, are well known and have been here recalled only for a better understanding of the numerical procedures applied throughout the present analysis both illustrated in the next section with the aid of a geometric, more intuitive, interpretation.

2.2. The FE-based limit analysis

The promoted FE-based procedure arises from the application of two different methods, namely the Elastic Compensation Method (ECM) and the Linear Matching Method (LMM), see e.g. [18], and references therein.

The ECM is aimed at determining the maximum value of loads, say $P_{LB}\,\bar{\mathbf{p}}$, in equilibrium with a plastically admissible stress field, at which the structure find itself at a state of incipient collapse. It then operates in the spirit of the static approach. The key-concept of the ECM is to *mimic the stress redistribution* arising within a structure approaching its critical (collapse) state when subjected to loads increasing up to collapse. Indeed the greater are the acting loads the wider are the structure portions where the elastic (plastically admissible) stresses attain an admissible threshold given by the assumed yield condition. When such redistribution cannot take place anymore the structure enters its post-elastic (plastic in this context) phase and plastic collapse is readily manifested. Precisely, the load increase is achieved by the ECM performing *many sequences* of elastic FE analyses. At the end

of each sequence the applied loads, say $P^{(s)}\,\bar{\mathbf{p}}$, with $P^{(s)}$ = load multiplier of the current sequence (s), is increased of a fixed increment. On the other hand, the stress redistribution is achieved by the ECM performing, for the current fixed loads $P^{(s)}\,\bar{\mathbf{p}}$ of the sequence, a number of FE analyses on the discretized structure in which a reduction of the elastic modulus is applied to the portions where the stress has attained the yield threshold.

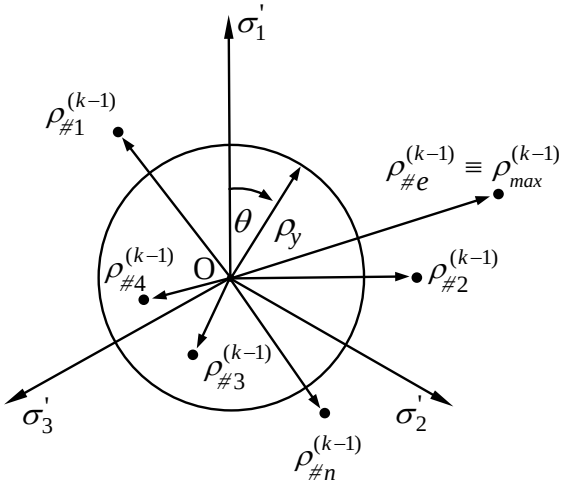

Figure 1: Von Mises circle in deviatoric plane. Geometrical sketch of the scalar-value stresses measured within the elements #1, #2, #3, ..., #e, ..., #n computed at iteration $(k-1)$ by the ECM. $\rho_{max}^{(k-1)}$ denotes the "maximum stress" among all the elements in the mesh.

The redistribution of the stresses associated to $P^{(s)}\,\bar{\mathbf{p}}$ is pursued iteratively and can be easily understood with reference to the sketch of Fig.1 where the assumed von Mises yield surface in the deviatoric $\pi-$plane is given by a circle of equation $\rho^2-\rho_y^2=0$, with $\rho:=\sqrt{2J_2}$ (being J_2 the second deviatoric stress invariant) and $\rho_y:=\sqrt{\frac{2}{3}}\sigma_y$ (being σ_y the uniaxial yield stress) is the

circle's radius.

The sketch of Fig.1 depicts the scalar value stresses computed at the $(k-1)$th iteration (or, equivalently, at the $(k-1)$th FE analysis within the current sequence) at each element in the FE mesh. Such value, say $\rho_{\#e}^{(k-1)}$ for the generic element $\#e$, is the average of the stress values computed at each Gauss point within the element. Among all the $\rho_{\#e}^{(k-1)}$ (with $\#e = 1, 2, ...$ total number of elements), the "maximum stress" in the whole mesh, named $\rho_{max}^{(k-1)}$ in Fig.1, is detected. Such a stress point is, in practice, the stress point "farthest away" from the von Mises circle. If such maximum value is greater than ρ_y, as hypothesized in the sketch, the method tries to redistribute the current loads $P^{(s)}\,\bar{\mathbf{p}}$ performing a new (kth) FE analysis of the discretized strucuture where within the elements with a $\rho_{\#e}^{(k-1)}$ greater than ρ_y (like, for example, in elements $\#1, \#2, \#e, \#n$, in Fig.1) the elastic modulus is *reduced*, *to bring* the not admissible stress onto the yield surface, according to the formula:

$$E_{\#e}^{(k)} = E_{\#e}^{(k-1)} \left[\frac{\rho_y}{\rho_{\#\,e}^{(k-1)}} \right]^2 . \tag{2}$$

If conversely, $\rho_{max}^{(k-1)}$ is less than ρ_y, circumstance not sketched but obviously met if all the $\rho_{\#e}^{(k-1)}$ stress points lay inside or onto the yield surface, compute a lower bound multiplier as:

$$P_{LB}^{(k-1)} = \rho_y \frac{P^{(s)}}{\rho_{max}^{(k-1)}}, \tag{3}$$

increase the intensity of the acting loads and perform a new sequence of elastic analyses in the attempt to redistribute a greater load. The sequences stop when the load increase does not allow the maximum stress to be brought below, or at, yield by redistribution. The P_{LB} is then the last computed value

corresponding to the last (maximum) redistributed admissible stress field.

The second method of the promoted procedure is, as said, the LMM. This method is aimed at determine an upper bound, say $P_{UB}\,\bar{\mathbf{p}}$, to the plastic collapse load of the structure so it follows the kinematic approach of limit analysis. The upper bound multiplier is computed in the shape given by Eq.(1), which can be rephrased with reference to the adopted von Mises circle in the deviatoric plane as:

$$P_{UB} = \frac{\int_V \rho_y \, \dot{\varepsilon}_d^c \, dV}{\int_{S_t} \bar{p}_i \, \dot{u}_i^c \, dS_t}. \tag{4}$$

In Eq.(4): $\dot{\varepsilon}_d^c$ is the deviatoric (plastic) strain rate at collapse having the direction of the outward normal to the von Mises circle at $\rho = \rho_y$; $\dot{u}_i^c$ are the related compatible displacement rates of the points where reference external loads $\bar{p}_i$, all collected in the vector $\bar{\mathbf{p}}$, act; ρ_y is the deviatoric stress invariant at yield (given by the radius of the von Mises circle in $\pi-$plane); $P_{UB}\,\bar{\mathbf{p}}$ are the acting loads. The integrals of Eq.(4) are numerically evaluated on the Gauss points within the element in which the structure is discretized or along the elements' side at the domain borders. The key-concept of the LMM is to *build a collapse mechanism* (plastic in this context), i.e. a velocity field in which the deformation is concentrated at points, lines, or planes, with the remaining parts of the system moving as rigid bodies. Looking again at Eq.(4) such collapse mechanism is given by the set $(\dot{\varepsilon}_d^c, \dot{u}_i^c)$. Once again we will refer to a geometric interpretation to explain the method that builds the collapse mechanism performing, at difference with the previous one, just *one sequence of linear analyses* on the structure discretized in FEs. Moreover, in this case the structure is made, by hypothesis, of a *linear viscous incompressible fictitious material with spatially varying Young modulus*. Such

assumption is indeed the artifice to build the collapse mechanism of the real structure operating on a *fictitious* one, i.e. a structure having the same geometry, boundary and loading conditions of its real counterpart but made of a material, with the above specified qualities, and fictitious in the sense that its elastic modulus may assume different values at different points, the latter being the Gauss points (GPs) in a FE model.

Once clarified in which sense the material is fictitious, a crucial remark concerns the required *linear viscosity* of it. First of all it is worth noting that for a linear viscous material the (viscous) strain *rates* can be expressed as partial derivatives, with respect to the stresses, of the pertinent *complementary dissipation rate functional*, say W, in the shape $\dot{\boldsymbol{\varepsilon}} = \partial W/\partial \boldsymbol{\sigma}$. The postulated linear viscosity of the fictitious material will then allow to compute, or express, the searched strain rates at collapse in terms of a defined functional W. On the other hand, the formal analogy existing between the linear viscous problem and the linear elastic one, will also allow to evaluate the above *fictitious viscous strain rates* as *fictitious finite elastic strains* viewing at the functional W as at the *complementary energy density functional* of a fictitious *elastic* material. This simplifies the procedure, allowing to perform a sequence of linear *elastic analyses* on the fictitious discretized structure. A final remark is related to the postulated incompressibility of the fictitious material. Under this hypothesis the complementary energy density of the fictitious material, in terms of deviatoric stress invariant ρ, can be given the simple shape:

$$W = \frac{3\,\rho^2}{4E}. \tag{5}$$

The latter, rewritten in the form $W = \bar{W} = \text{constant}$, defines in the deviatoric $\Pi-$plane a *complementary energy equipotential surface* in the shape of a circle centered at the origin with radius equal to $2\sqrt{\frac{\bar{W}E}{3}}$, a circumstance useful for the rationale that follows.

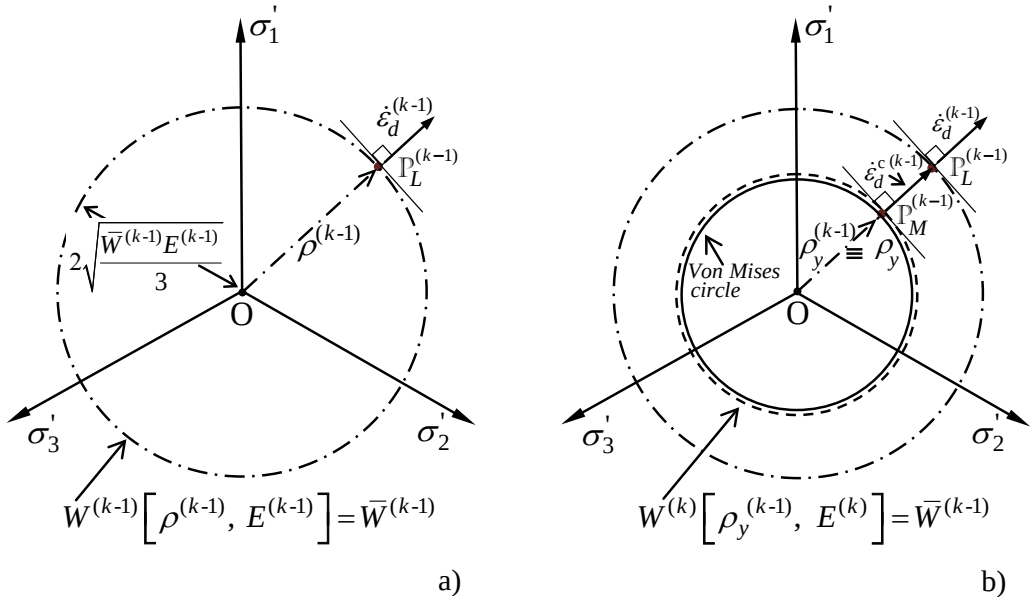

Figure 2: Geometrical sketch of the LMM at a generic Gauss point in the FE mesh and at iteration $(k-1)$: a) fictitious solution $\mathbb{P}_L^{(k-1)}$ onto $W^{(k-1)} = \bar{W}^{(k-1)}$; b) rescaling of $W^{(k-1)} = \bar{W}^{(k-1)}$ to $W^{(k)} = \bar{W}^{(k-1)}$ through modification of the fictitious Young modulus to match the von Mises circle at $\mathbb{P}_M^{(k-1)}$ for given $\dot{\varepsilon}_d^{(k-1)} \equiv \dot{\varepsilon}_d^{c(k-1)}$.

With reference to Fig.2(a), let us expound the LMM that, as said, performs *one* sequence of elastic FE analyses on the above defined fictitious structure. For clarity we focus the attention on one generic GP of the FE mesh and at the current, say $(k-1)$th, iteration, or FE analysis of the sequence. At the beginning, say for $k = 1$, the fictitious material has a Young modulus $E^{(0)}$ equal, at all GPs, to an arbitrary value that can also be the

real value. The fictitious solution obtained, at the focused GP, under given loads $P^{(k-1)}\bar{p}_i$ can be represented, as sketched in Fig.2(a) on $\Pi-$plane, as a stress point, say $\mathbb{P}_L^{(k-1)}$, lying on the complementary energy equipotential surface $W^{(k-1)}\left[\rho^{(k-1)}, E^{(k-1)}\right] = \bar{W}^{(k-1)}$ referred to the fictitious material. As suggested in the sketch the stress point $\mathbb{P}_L^{(k-1)}$ is located by the computed deviatoric stress invariant $\rho^{(k-1)}$ while the outward normal at $\mathbb{P}_L^{(k-1)}$ is, for the postulated incompressibility of the fictitious material, the associated deviatoric strain rate $\dot{\varepsilon}_d^{(k-1)} = \partial W^{(k-1)}/\partial\rho^{(k-1)}$ compatible with the computed (fictitious) displacement rates $\dot{u}_i^{(k-1)}$. It is worth noting that, based on the recalled analogy between a linear viscous material and a linear elastic one, the above *rates* quantities are computed as *finite* (elastic) quantities. It is also worth noting that the wideness of the circle $W^{(k-1)} = \bar{W}^{(k-1)}$ depends from the current value of $E^{(k-1)}$ and $\bar{W}^{(k-1)}$. The latter, at $k = 1$, is given by $\bar{W}^{(0)} = (3/4)\ \left[\rho^{(0)}\right]^2 / E^{(0)}$.

Aside from this obvious geometric interpretation, useful for the following rationale, the fictitious solution is eventually given by $\rho^{(k-1)}$, in equilibrium with loads $P^{(k-1)}\,\bar{p}_i$, together with an associated $\dot{\varepsilon}_d^{(k-1)}$ compatible with $\dot{u}_i^{(k-1)}$. Looking again at Eq.(4) it is easy to realize that if the fictitious solution is "forced to become a solution at yield", i.e. if $\mathbb{P}_L^{(k-1)}$ is brought onto the von Mises yield surface of the real material we have all the *ingredients* to compute a P_{UB} in the shape of Eq.(4). To explain this crucial action of the LMM we refer to the sketch of Fig.2(b), focusing again on the stress state of the generic GP and referring to the $\Pi-$plane where the von Mises yield surface of the real material and the complementary energy equipotential surface of the fictitious one, $W^{(k-1)}[\rho^{(k-1)}, E^{(k-1)}] = \bar{W}^{(k-1)}$, are homothetic circles

centered at the origin. To *bring* $\mathbb{P}_L^{(k-1)}$ onto von Mises surface it suffices to modify the fictitious elastic modulus *at the focused GP* with the formula:

$$E^{(k)} = E^{(k-1)} \frac{\rho_y}{\rho^{(k-1)}}, \tag{6}$$

so rescaling the surface $W^{(k-1)} = \bar{W}^{(k-1)}$. The hypothesized $\mathbb{P}_L^{(k-1)}$ in Fig.2(b) (out of the von Mises circle) entails a reduction of $W^{(k-1)} = \bar{W}^{(k-1)}$ but if $\mathbb{P}_L^{(k-1)}$ was inside the von Mises circle the rescaling of $W^{(k-1)} = \bar{W}^{(k-1)}$ would be an increase. Eventually the rescaled surface $W^{(k)}\left[\rho_y^{(k-1)} \equiv \rho_y, E^{(k)}\right] = \bar{W}^{(k-1)}$ *coincides* or, *matches*, the yield surface at point $\mathbb{P}_M^{(k-1)}$, the latter representing a solution at yield in terms of $\rho_y^{(k-1)} \equiv \rho_y$, with associated $\dot{\varepsilon}_d^{c(k-1)} \equiv \dot{\varepsilon}_d^{(k-1)}$ compatible with the $\dot{u}_i^{c(k-1)} \equiv \dot{u}_i^{(k-1)}$.

If the expounded *modulus variation* is *repeated at all GPs* of the mesh, a collapse mechanism $\left(\dot{\varepsilon}_d^{c(k-1)}, \dot{u}_i^{c(k-1)}\right)$ with related stresses at yield $\rho_y^{(k-1)} \equiv \rho_y$ can be defined for the whole structure and, by Eq.(4), an upper bound to the plastic collapse load multiplier, say $P_{UB}^{(k)}$, can be evaluated at current $(k-1)$th analysis as:

$$P_{UB}^{(k)} = \frac{\int_V \rho_y^{(k-1)}\, \dot{\varepsilon}_d^{c(k-1)}\, dV}{\int_{S_t} \bar{p}_i\, \dot{u}_i^{c(k-1)}\, dS_t}. \tag{7}$$

It is worth noting that the above *stress at yield*, $\rho_y^{(k-1)} \equiv \rho_y$, has been *generated*, at each GP, *by* the described *matching procedure*, i.e. *geometrically*. Such stresses do not meet equilibrium conditions with the acting loads $P^{(k-1)}\,\bar{p}_i$ and the procedure is iterative. At iteration (k) the analysis will be carried on with the updated $E^{(k)}$ computed at iteration $(k-1)$th and under loads $P_{UB}^{(k)}\,\bar{p}_i$. The iterations stop when the difference between two subsequent P_{UB} values is less than a fixed tolerance. Two further final

remarks necessitate on the LMM, which has been applied by the Authors with reference to different yield criteria, see again [14], [18]. The first remark concerns a *sufficient condition for convergence* of the entire procedure here fully met and addressed in [21]. The second remark concerns the circumstance that the computed upper bound *converges* monotonically *to the least upper bound* allowed by the adopted mesh geometry and shape functions, a matter addressed in [22] where the method was first conceived. Both matters are out of the scope of the present study and the interested Reader can refer to the above quoted papers for a deeper comprehension.

3. Experimental results versus numerical predictions

3.1. Experimental test set up

The laboratory tests reported in [19] have been considered as benchmark for validating the discussed limit analysis numerical procedure facing experimental findings on real scale prototypes. The tests were there mainly oriented to appraise experimentally the behavior of welded beam-to-column steel joints suffering cyclic loads and to compare some of the more common damage models and failure criteria available in the literature. The main goal was indeed to assess the capability of available models/criteria to correctly interpret the actual cyclic behavior of critical parts of a steel structural organism, both in terms of deterioration of their mechanical properties and of energy absorption capacity. Nevertheless, two of the examined specimens, precisely the ones named BCC5-E and BCC6-E, were also tested up to collapse under a monotonically increasing load. The tests were actually stopped when the recorded load-displacement diagram was exhibiting a sub-horizontal

trend witnessing an incipient plastic collapse at a constant load. These two are the tests hereafter analyzed for validation.

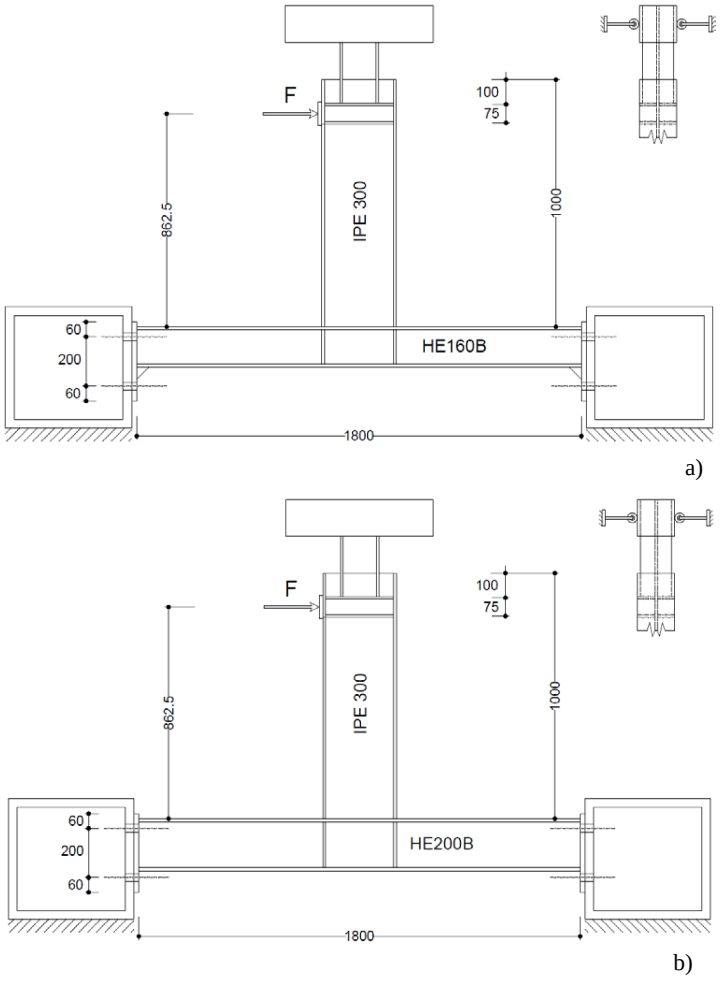

Figure 3: Geometry, boundary and loading conditions of the analyzed specimens: a) BCC5-E; b) BCC6-E.

Figures 3(a,b) report the geometry, boundary conditions, loading conditions of the two specimens respectively, giving also the main details of the test device shown in the pictures of Fig.4. Moreover, on the top right of Figs.3(a,b)

it is sketched a contrivance welded above the loaded point to the head of the IPE metal profiles to prevent out-of-plane deformations during tests.

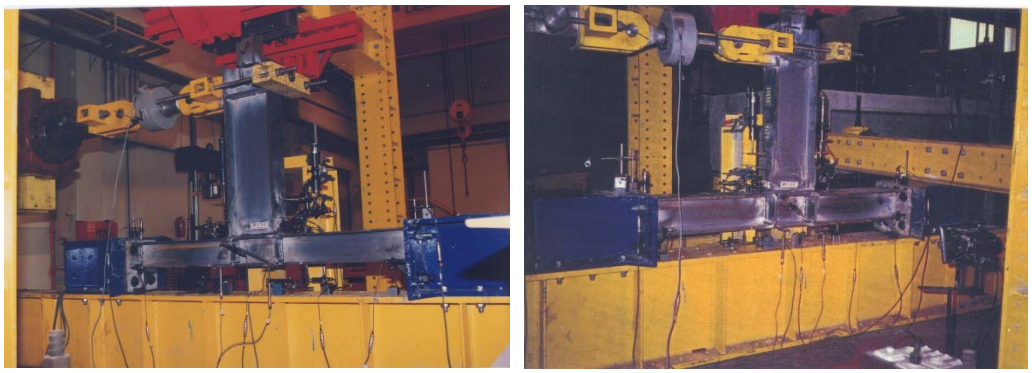

Figure 4: Pictures of the test device.

It is also worth noting that referring to a typical steel framed structure subjected to horizontal (seismic) actions, the qualitative bending moments diagrams are those sketched in Fig.5(a). As suggested in Fig.5(b) the joint has been tested in a configuration which is rotated anticlockwise of 90^0 with respect to its real working position when embedded in a steel frame. The horizontal elements in the tests (HE160B and HE200B) are actually the columns of the real joint, the vertical elements in the tests (IPE300) are the beams of the real configuration. Two hinges would have been more appropriate at the end sections of the HE metal profiles of the tested specimens instead of clamps, nevertheless, for our purposes, this circumstance does not affect the validity of the numerical simulation of the tests in which the actual test boundary conditions (clamps) have been applied to the FE model. Tables 1 and 2 give the actual (measured) dimensions and the yield stress values of

the metal profiles of the two specimens.

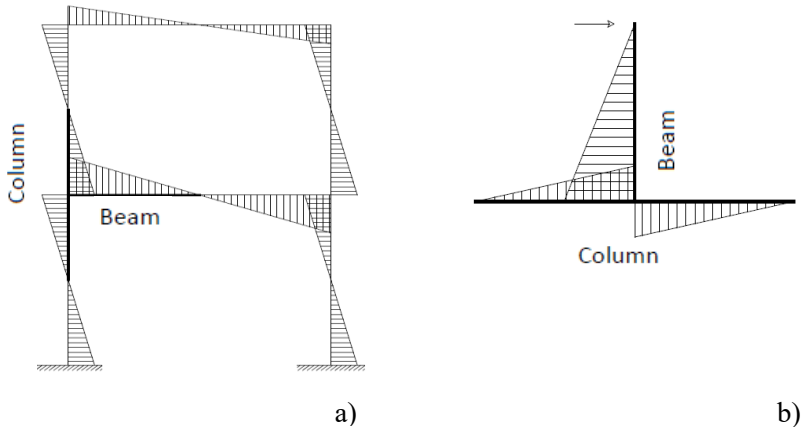

Figure 5: Analyzed beam-to-column steel joint: a) real configuration of the joint embedded in a typical steel frame; b) laboratory test configuration.

Finally, Figures 6(a,b) report the experimentally detected load-displacement curves. It is worth noting that the $F-d$ curve obtained for specimen BCC6-E shows an abrupt change in the curve slope at $F = 239.62$kN. This was due to the formation of a crack in the beam flange close to the weld line, i.e. located within the so-called Heat-Affected Zone. A consequent local buckling of the beam flange under compression caused the loss of the member's load-carrying capacity and the premature interruption of the test. However, looking at the results of BCC5-E and estimating a possible position of the plastic plateau for specimen BCC6-E, it seems sensible to assume that the correct experimental load-displacement curve would have given a plastic collapse load of about 258kN. The dashed-lines in Figs.6(a,b) indicate the experimentally detected values of the plastic collapse load equal to 228kN for BCC5-E and, with the

Metal profile	**IPE 300**	**HE 160 B**
Geometry [mm]		
Height	299.0	162.5
Width	151.0	162.0
Flange thickness	10.3	13.0
Web thickness	7.2	8.9
Yield stress [MPa]		
Flange	274.78	323.13
Web	305.54	395.56

Table 1: Actual (measured) geometrical dimensions and yield stress of the beam-to-column joint metal profiles of specimen BCC5-E (steel S235)

.

Metal profile	**IPE 300**	**HE 200 B**
Geometry [mm]		
Height	298.5	201.0
Width	151.0	200.0
Flange thickness	10.6	14.5
Web thickness	7.0	9.8
Yield stress [MPa]		
Flange	278.62	312.55
Web	304.92	401.62

Table 2: Actual (measured) geometrical dimensions and yield stress of the beam-to-column joint metal profiles of specimen BCC6-E (steel S235)

.

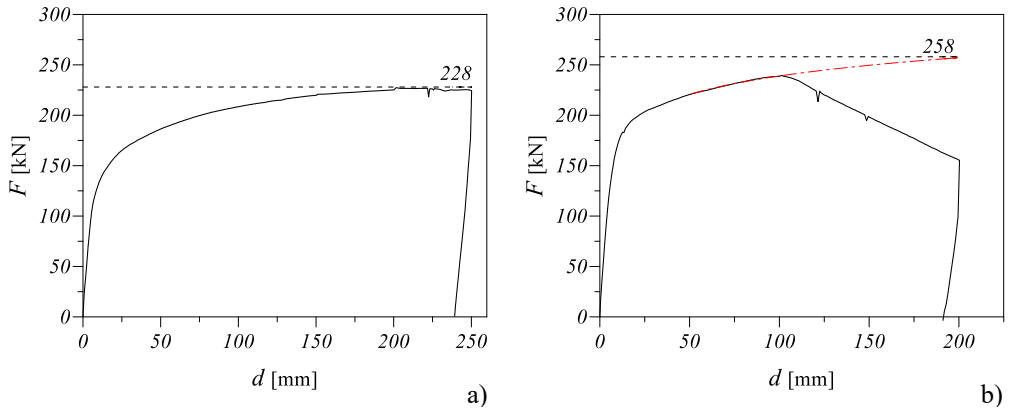

Figure 6: Load-displacement experimentally detected curves: a) specimen BCC5-E; b) specimen BCC6-E. Dashed-lines denote the plastic collapse load experimental value.

declared approximation, equal to 258kN for BCC6-E.

3.2. Numerical simulations

The experimental tests described in the previous section have been numerically simulated applying the promoted procedure to predict the plastic collapse load for each specimen. A FORTRAN main code drives the commercial code ADINA, which carries on all the elastic analyses required by the ECM and by the LMM.

More specifically, a first FORTRAN segment governs the sequences of the FE elastic analyses of the ECM, increases the multiplier of the reference load at the end of each sequence, redistributes the acting loads of the current sequence driving the iterative FE analysis within the sequence. Indeed, at each iteration (analysis) the Young modulus of the FEs where the computed (deviatoric) stress $\rho_{\#e}$ is greater than a known threshold is reduced according to Eq.(2). Finally, such first FORTRAN segment computes a lower bound

multiplier, in the shape given by Eq.(3), at the end of each successful sequence, i.e. a sequence characterized by a re-distributable load. It stops the sequences when the maximum re-distributable load is reached.

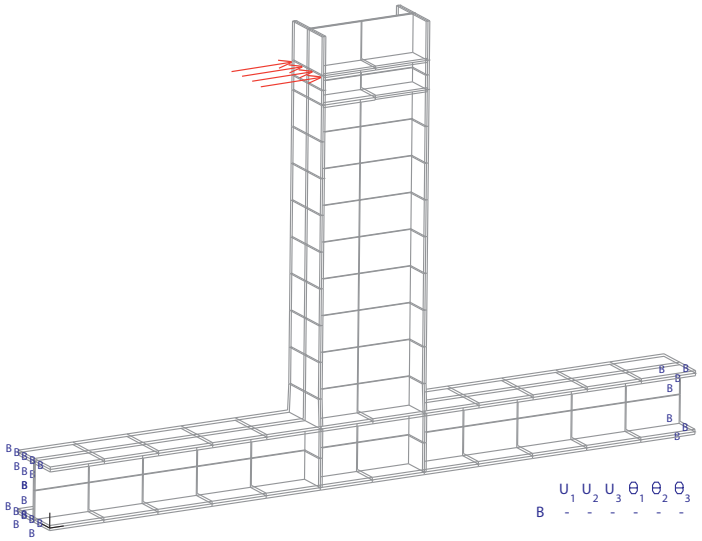

Figure 7: FE meshes, boundary and loading conditions of a typical mesh adopted.

A second FORTRAN segment governs the sequence of the fictitious elastic analyses of the LMM. It actually starts with a first FE analysis of the discretized structure with a Young modulus initial value equal at all GPs of the mesh. It then accomplishes the matching procedure at each GP of the mesh so modifying the Young modulus value at the GP according to Eq.(6). It computes an upper bound according to Eq.(7) and feeds the ADINA elements with the modified (fictitious) Young modulus values (a unique value obtained averaging among the GPs of the element is used) to perform a new analysis under loads amplified by the computed upper bound till equilibrium is satisfied.

Figure 7 shows the FE mesh adopted for the analysis of the two specimens BCC5-E and BCC6-E. Shell-type ADINA elements with 8 nodes, 6DOF per node and 9 GPs have been adopted to perform numerical integrations. The DOFs of all FEs nodes, out of the plane of structural symmetry, have been impeded for a consistent numerical simulation. More precisely, a mesh of 160 FEs has been used for both specimens. The hypothesis of incompressibility of the fictitious material, required by the LMM, has been obtained assuming a computationally acceptable value of the Poisson ratio equal to 0.4999

Figures 8(a,b) show the computed values of the upper and lower bound multipliers to the plastic collapse load versus iteration number for the P_{UB} and versus iteration number at last successful sequence for the P_{LB}; both are plotted against the experimentally detected plastic collapse load multiplier, P_{EXP}. All the multipliers are given assuming the experimentally detected plastic collapse load as reference load, so P_{EXP} is equal to 1. It is worth noting that the numerical bounds are reached in few iterations/sequences and with a monotonic convergence. Despite the coarse meshes adopted, the two bounds locate the real collapse multiplier within a pretty narrow band witnessing the effectiveness of the whole procedure.

The coincidence of P_{UB} and P_{LB} with $P_U \equiv P_{EXP}$, claimed by the theory of limit analysis for standard materials, could be obtained numerically with finer meshes. To this concern, specimen BCC5-E has been analyzed once again with the finer mesh (650 FEs) of Fig.9 with a mesh refinement around the welded zone of the joint. The related P_{UB} and P_{LB} values are plotted against the iterations in Fig. 10. By inspection of the plotted curves the following remarks can be drawn: i) the two bounds get very close to each other

with a difference of 6%, which seems acceptable in terms of "coincidence" of two numerical solutions. They eventually give in practice a "unique" value of the plastic collapse load as required by the theory for a standard perfectly plastic material; ii) the P_{UB} shows a significative improvement getting closer to the final experimentally detected plastic limit value. No significative gain is obtained for the P_{LB}. From this point of view the LMM seems more accurate. To this concern it is worth noting that to adopt a finer mesh implies an enrichment of the kinematic description of the structural FE model, a circumstance directly influencing the kinematic approach on which the LMM is based. No such advantage is gained in terms of stress description with a mesh refinement, and this is the reason of no significative variation of the ECM results. Eventually, the analysis carried on with a finer mesh, computationally more cumbersome, appears not useful from a practical point of view.

A second, but not secondary, useful result concerns the possibility offered by the promoted numerical procedure of locating the plasticized zones at collapse as shown in Figures 11(b) and 12(b) for the two specimens and the coarse mesh.

The contour plots of the strain components along the plane of loading, pertaining to the plastic collapse mechanism built by the LMM at last converged iteration, give indeed such information. The latter, even if qualitative —the plotted quantities have to be interpreted for what they are, i.e. plastic strain *rates* at collapse, or *directions* of plastic strains— can be very useful to localize critical zones or weaker members within structures of large dimensions. Moreover, the above contour plots are given in Figures 11(b) and 12(b) on

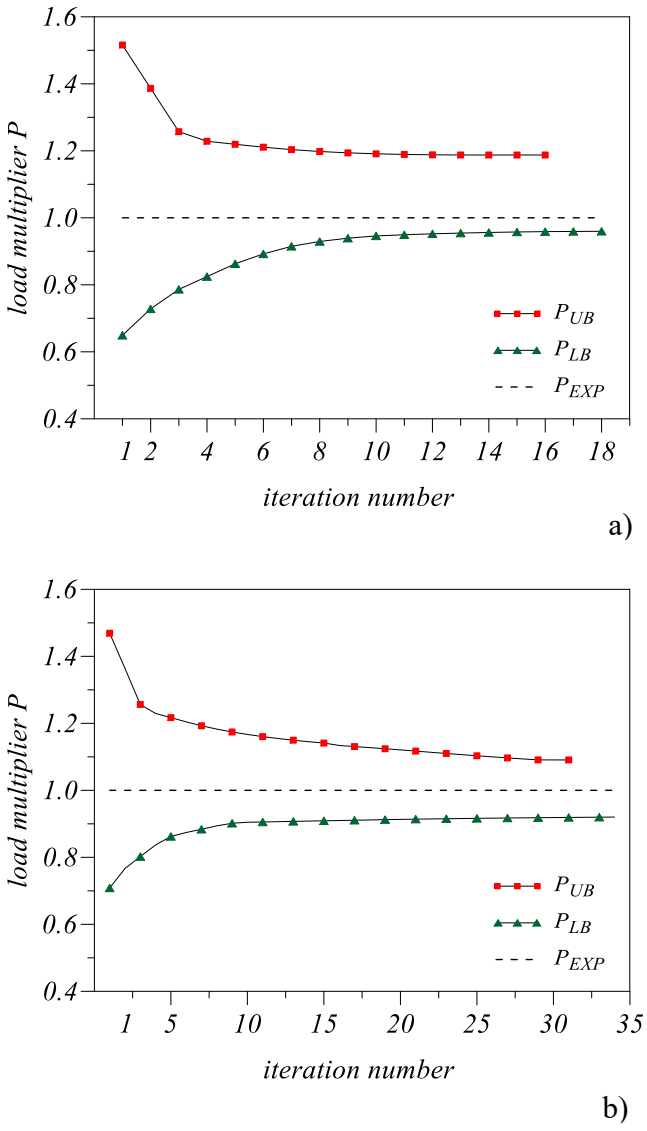

Figure 8: Plastic collapse load multipliers. Solid line with squares plots the upper bound values (P_{UB}) versus iteration number; solid line with triangles plots the lower bound values (P_{LB}) versus iteration number at last successful sequence; dashed line denotes the experimentally detected plastic collapse load multiplier (P_{EXP}): a) specimen BCC5-E, b) specimen BCC6-E.

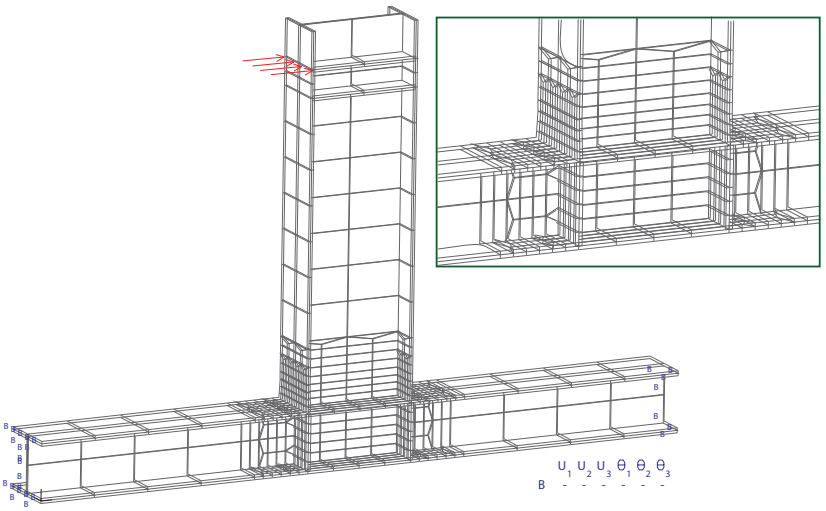

Figure 9: Finer FE mesh of specimen BCC5-E, boundary and loading conditions.

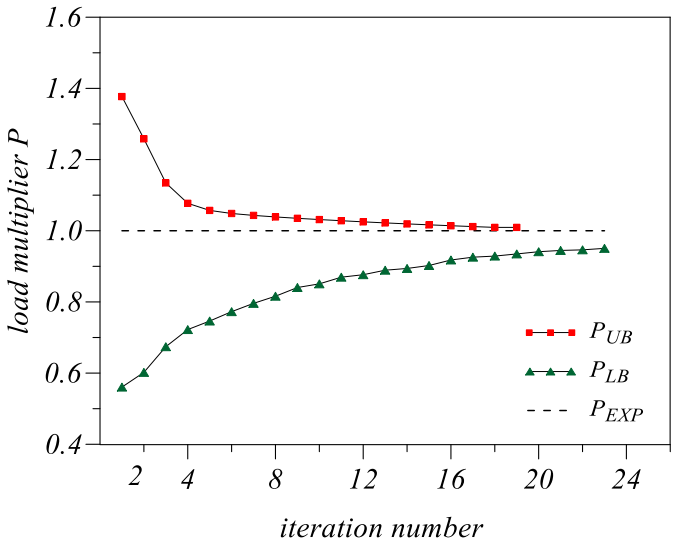

Figure 10: Plastic collapse load multipliers for specimen BCC5-E analyzed with the finer mesh of Fig.9. Solid line with squares plots the upper bound values (P_{UB}) versus iteration number; solid line with triangles plots the lower bound values (P_{LB}) versus iteration number at last successful sequence; dashed line denotes the experimentally detected plastic collapse load multiplier (P_{EXP}) .

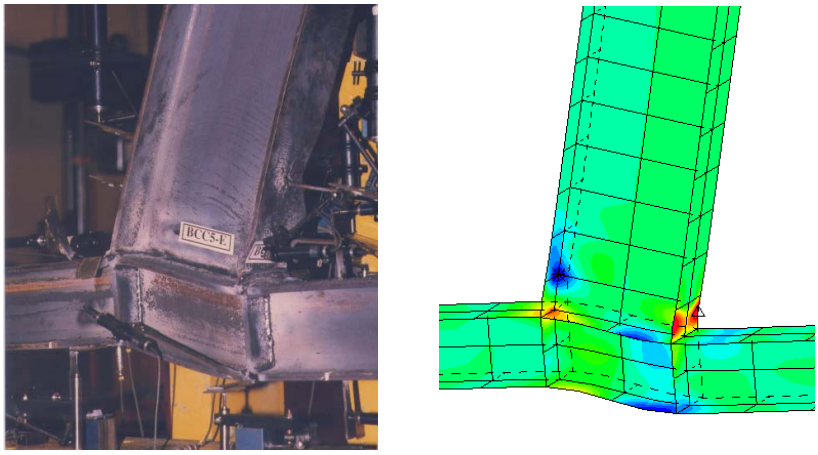

Figure 11: Specimen BCC5-E at collapse: a) experimentally observed plastic collapse mechanism; b) deformed mesh and contour plots of the strain components along the plane of loading at last (converged) iteration of the LMM.

the deformed discretized structures, i.e. the ones obtained by applying the computed displacement rates at collapse ($\dot{u}_i^c$) at all nodes of the meshes. The comparison with the experimental evidences, shown in the pictures of Figures 11(a) and 12(a), is impressive also showing the capability of the procedure of predicting the plastic collapse mechanism shape. By inspection of Figs. 11(b) and 12(b) it appears how, beyond the plasticized zones, the deformed meshes at collapse locate also the parts of the structure which rotate rigidly, as it happened experimentally and as it has to be when a structure undergoes plastic collapse. Finally, Figures 13(a,b) show the contour plots of the plastically admissible stresses given by the ECM at last successful sequence. Also these results, quantitative this time —being stresses in equilibrium with the maximum re-distributable load— but not verifiable experimentally, seem to validate the good predictive capabilities of the procedure.

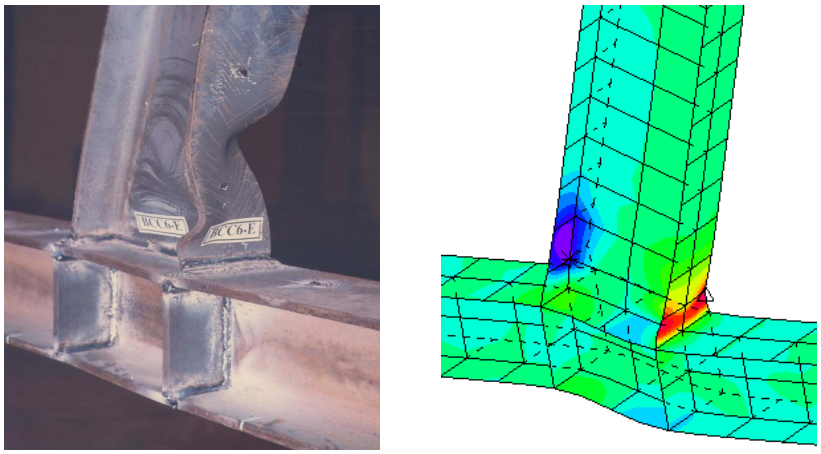

Figure 12: Specimen BCC6-E at collapse: a) experimentally observed plastic collapse mechanism; b) deformed mesh and contour plots of the strain components along the plane of loading at last (converged) iteration of the LMM.

4. Concluding remarks and future developments

The main findings and possible steps forwards of the present study can be summarized as follows:

A numerical FE-based procedure for limit analysis has been applied for predicting the plastic collapse load as well as the plastic collapse mechanism of two real scale prototypes of beam-to-column steel joints tested up to collapse. The obtained results seem to confirm the fair predictive capabilities of the procedure already experienced in different contexts but here rephrased in a very simple and effective way with reference to von Mises material in the deviatoric plane. Avoiding enthusiastic conclusions, being other checks necessary, the expounded methodology seems applicable straightforward to the

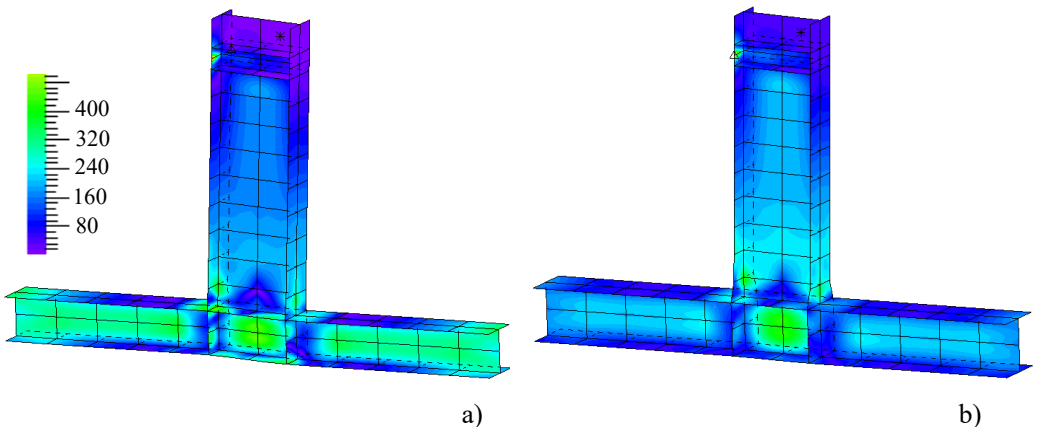

Figure 13: Contour plots of plastically admissible stresses computed by the ECM at last successful sequence: a) specimen BCC5-E; b) specimen BCC6-E.

analysis of more complex structures characterized by structural components made of many different materials with a post-elastic behaviour not easy to handle or not uniquely defined. In such context the limit load evaluation is still more reliable and competitive with respect to step-by-step nonlinear analyses.

The application to composite steel-concrete structures and to concrete-filled welded steel columns are, among others, next possible steps of the present approach and are the object of an ongoing research.

References

[1] Maheri M.R., Sahebi A. Use of steel bracing in reinforced concrete frames. Engineering Structures 1997; 2(12): 1018-1024.

[2] Oinam R.M., Sahoo D.R. Seismic rehabilitation of damaged reinforced

concrete frames using combined metallic yielding passive devices. Structure and Infrastructure Engineering 2017; 13(6): 816-830.

[3] Di Sarno L., Elnashai A.S. Seismic retrofitting of steel and composite building structures. Report02-01. Mid-America Earthquake Center, Civil and Environmental Engineering Department, University of Illinois at Urbana-Champaign 2002.

[4] D'Ayala D., Galasso C., Minas S., Novelli V. Review of retrofitting methods to reduce seismic vulnerability of buildings, with particular reference to hospital and medical facilities. doi:10.12774/eodhdr.june2015.ddayalaetal1, July 2015.

[5] Oehlers D.J., Bradford M.A. Composite steel and concrete structural members. Fundamental behaviour. Pergamon, 1th ed. 1995.

[6] Spacone E., El-Tawil S. Nonlinear analysis of Steel-Concrete Composite Structures: State of the Art. Journal of Structural Engineering 2004; 130(2): 159-168.

[7] Ekmekyapar T. Experimental performance of concrete filled welded steel tube columns. Journal of Constructional Steel Research 2016; 117: 175-184.

[8] Khanouki M.M.A., Sulong N.H.R., Shariati M., Tahir M.M. Investigation of through beam connection to concrete filled circular steel tube (CFCST) column. Journal of Constructional Steel Research 2016; 121: 144-162.

[9] Liu S-W., Chan T-M., Chan S-L, So D.K-L. Direct analysis of high-strength concrete-filled-tubular columns with circular & octagonal sections. Journal of Constructional Steel Research 2017; 129: 301-314.

[10] Huang W., Fenu L., Chen B., Briseghella B. Experimental study on K-Joints of concrete-filled steel tubular truss structures. Journal of Constructional Steel Research 2015; 107: 182-193.

[11] Liu R., Liu Y. Analysis of auxiliary ribs in steel-concrete joint of hybrid girder. Journal of Constructional Steel Research 2015; 112: 363-372.

[12] Vasdravellis G., Uy B., Tan E.L., Kirkland B. Behaviour and design of composite beams subjected to sagging bending and axial compression. Journal of Constructional Steel Research 2015; 110: 29-39.

[13] Yu T., Hu Y.M., Teng J.G. Cyclic lateral response of FRP-confined circular concrete-filled steel tubular columns. Journal of Constructional Steel Research 2016; 124: 12-22.

[14] Pisano, A.A., Fuschi, P. Mechanically fastened joints in composite laminates: Evaluation of load bearing capacity. Composites Part B: Engineering 2011; 42(4): 949-961.

[15] Pisano A.A., Fuschi P., De Domenico D. A layered limit analysis of pinned-joints composite laminates: Numerical versus experimental findings. Composites: Part B 2012; 43: 940-952.

[16] Pisano A.A., Fuschi P., De Domenico D. Failure modes prediction of multi-pin joints FRP laminates by limit analysis. Composites Part B: Engineering 2013; 46: 197-206.

[17] De Domenico D., Pisano A.A., Fuschi P. A FE-based limit analysis approach for concrete elements reinforced with FRP bars. Composite Structures 2014; 107: 594-603.

[18] Pisano A.A., Fuschi P., De Domenico D. Limit analysis on RC-structures by a multi-yield-criteria numerical approach. In: Direct Methods for Limit and Shakedown Analysis of Structures: Advanced Computational Algorithms and Material Modelling, Fuschi P., Pisano A.A., Weichert D. Eds., Springer International Publishing 2015.

[19] Castiglioni C., Pucinotti R. Failure criteria and cumulative damage models for steel components under cyclic loading. Journal of Constructional Steel Research 2009; 65: 751-765.

[20] Lubliner J. Plasticity theory. Macmillan Publishing Company, New York, 1990.

[21] Ponter A.R.S., Fuschi P., Engelhardt M. Limit analysis for a general class of yield conditions. European Journal of Mechanics/A Solids 2000; 19: 401-421.

[22] Ponter A.R.S., Carter K.F. Limit state solutions based upon linear elastic solutions with spatially varying elastic modulus. Computer Methods Appl Mech Eng 1997; 140: 237-258.